

Brain Resonance Imaging Segmentation Method Based on Deep ResUNet

Wenxin Yang

Changchun University of Science and Technology, College of Computer Science and Technology,
Changchun, Jilin 130022

Abstract. The present invention discloses a cathode frame of an electrostatic precipitator, comprising a rectangular frame composed of four horizontal bars and five vertical bars; The horizontal and vertical bars are perpendicular to each other and located in the same plane, and four horizontal bars are arranged parallel to each other, while five vertical bars are arranged parallel to each other; Four horizontal bars divide the longitudinal length of the rectangular box into three equal parts, five vertical bars divide the transverse length of the rectangular box into 2:1:1:2, and one of the vertical bars is located on the vertical centerline of the rectangular box; The upper section of the two outermost vertical rods on the rectangular frame is a reinforced vertical rod, and there are two horizontal through-holes on the reinforced vertical rod for installing the cathode frame support. The cathode frame of the electrostatic precipitator has a simple structure and convenient assembly, which can effectively prevent the cathode frame of the electrostatic precipitator from bending, deformation, or even sliding and collapsing from the overall cathode support, greatly improving the safety and stability of the operation of the electrostatic precipitator.

Keywords: Electrostatic precipitator; Cathode frame; Anti bending deformation; Anti slip collapse; high safety and stability.

1. Introduction

With the rapid development of medical imaging technology in recent years, MRI has been a vital tool for clinical diagnosis and treatment[1], which can obtain high-definition images of human tissues by using the principle of nuclear magnetic resonance. Advantageous in non-invasiveness, non-radiation, and multi-dimensional information, it can provide detailed anatomical structure and pathological information. Due to the increasing MRI data, traditional manual analysis and interpretation have become time-consuming and prone to subjective errors [2].

Deep learning is a machine learning method based on neural network structure with excellent abilities in automatic learning and feature extraction[3]. For example, Chen Guoxiang [4] used it to recognize and diagnose X-ray images of COVID-19. Zhang Peng et al. [5] used it to detect and segment pulmonary nodules and diagnose canceration. Combining the spatiotemporal data, thus, processing MRI by deep learning can effectively conduct automatic analysis, feature extraction, and disease diagnosis [6].

When using deep learning for MRI target detection and segmentation, deep learning has made remarkable progress in all aspects [7]. For example, Res-Net is a neural network architecture in deep learning, which solves the gradient problem of traditional networks by introducing residual connections. It can directly transmit the input information to the following layers by introducing jumping connections between layers, so that the network can be trained deeper and easier [8]. As a neural network architecture for image segmentation, U-Net consists of an encoder and decoder [9]. The encoder contains a series of convolution layers and down-sampling operations, while the decoder contains a series of up-sampling operations and convolution layers. At each stage between the encoder and the decoder, U-Net connects their feature maps [10], which directly transmits the high-resolution feature map to the decoder through a skip connection to provide richer spatial information and contextual features. Res-Net and U-Net are widely used in the field of medical image segmentation.

Although deep learning has many achievements in MRI image processing, some problems such as low accuracy of image segmentation still exist. This paper combines ResUNet, a mixed model of

2.3 MRI Segmentation Method Based on ResUNet

Figure 3 shows the overall structure of ResUNet algorithm studied in this paper.

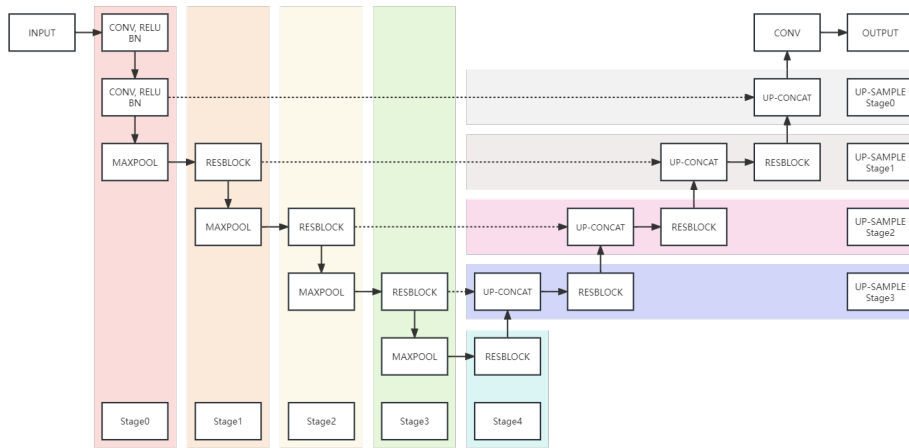


Figure 3 Network Model Structure of ResUNet

According to Figure 3, the ResUNet algorithm adopts the method of multi-model mixed nesting, that is, it adds a residual module based on U-Net, which enables it to make more comprehensive use of the original input information of MRI than U-Net. ResUNet algorithm can fully utilize advantages of Res-Net and U-Net through this structure design, so as to realize deep feature extraction and accurate image segmentation.

2.4 Model Evaluation Index

Positive and negative are usually used to represent two categories in the medical field. Positive means that a certain symptom exists or an abnormal index is detected, while negative means that the inspected symptom does not exist or the monitored index is not abnormal. Disease diagnosis is decision-making and classification of positive and negative, with the possible relationship between their state and decision shown in Table 1.

Table 1 Possible Relationship Between State and Decision

Decision-Making	State	
	Positive	Negative
Positive	True positive (TP)	False positive (FP)
Negative	False negative (FN)	True negative (TN)

In Table 1, TP represents the number of positives predicted as positives, TN is the number of negatives predicted as negatives, FP is the number of negatives predicted as positives, FN is the number of positives predicted as negatives. TP and TN are both correct predictions, while FN and FP are both incorrect.

Based on the confusion matrix, common evaluation indexes include Accuracy, Loss, Precision, Recall, G-mean, F1, and AUC (Area Under ROC Curve) as shown in formula2-6.

$$Acc = \frac{TP + TN}{TP + TN + FP + FN} \tag{2}$$

$$Rec = \frac{TP}{TP + FN} \tag{3}$$

$$Pre = \frac{TP}{TP + FP} \tag{4}$$

$$F1 = \frac{2Rec \cdot Pre}{Rec + Pre} \tag{5}$$

$$IoU = \frac{Area(C) \cap Area(G)}{Area(C) \cup Area(G)} \tag{6}$$

3. Experimental Process

3.1 Dataset and Data Preprocessing

The LGG segmentation dataset (<https://wiki.cancerimagingarchive.net/display/Public/TCGA-LGG>) is used in this paper to verify the effectiveness of the proposed ResUNet algorithm. LGG segmentation dataset includes brain MRI and FLAIR anomaly segmentation masks that are manually labeled, consisting of 110 patients, and widely used in medical research. The statistics of tumor presence or absence in MRI images in the LGG dataset are shown in Figure 4.

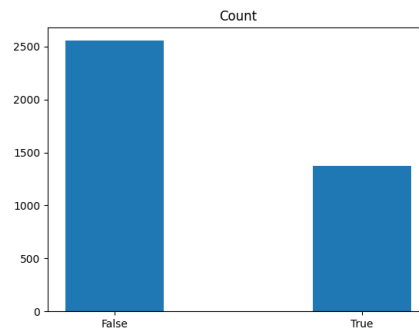


Figure 4 Statistics of Tumor Presence or Absence in Image Dataset

According to Figure 4, the images with tumors in the LGG segmentation dataset account for about 33% of the total. MRI images of patients in some datasets and corresponding artificial calibration images are randomly selected, with the comparison between normal images and abnormal images shown in Figure 5.

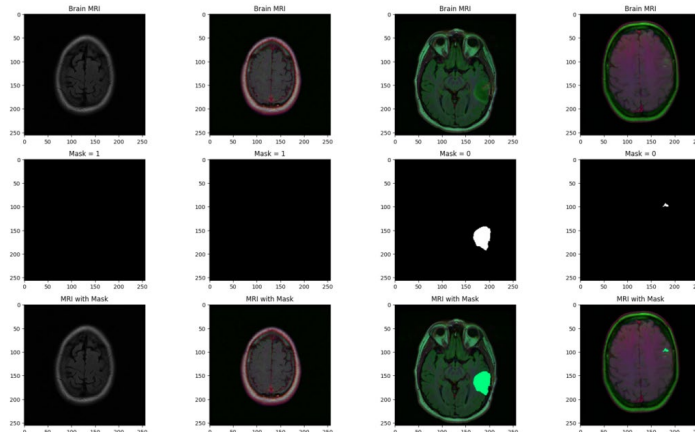


Figure 5 Statistics of Tumor Presence or Absence in Image Dataset

Each column is a randomly selected MRI image in Figure 5. The first two columns show normal MRI images without tumors and the last two show those abnormal with tumors. The first row shows the original MRI image, the second row shows the manually calibrated tumor area in the dataset, and the third row highlights the manually calibrated area in the original image. According to the output results, there is no tumor in the first two columns, so the first row is consistent with the third. Because of the tumor presence in the last two columns, a bright green area can be seen in the third row.

3.2 Target Recognition and Classification

According to the preprocessed dataset, the training and test sets are divided by splitting, and each structure of the U-Net network is added to the model output to form a composite network composed of 25,751,426 parameters, in which 53,120 untrainable parameters are removed. Besides, the training and test results are obtained after the training set trained for trainable 25,698,306 parameters shown in Figure 6.

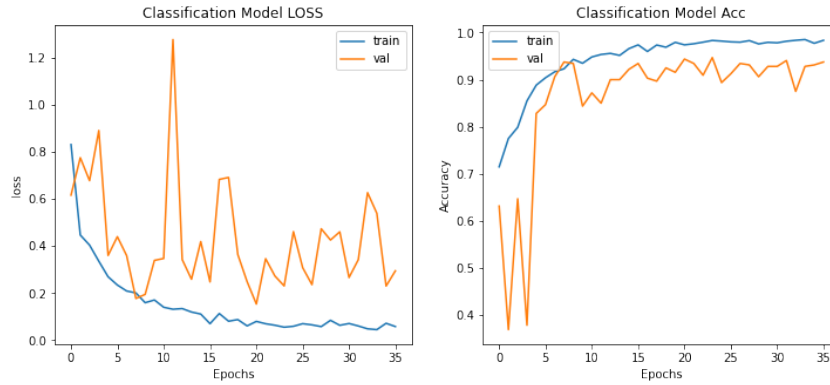


Figure 6 Training Details of Tumor Recognition and Classification Model

In the model evaluation stage, the model loss function in the training process and the model correct rate are obtained through the test set data. It can be seen that the model finally converges after several iterations in the training process and the correct rate of the model remains above 90% after convergence with high training effects. The confusion matrix of the recognition result is shown in Figure 7.

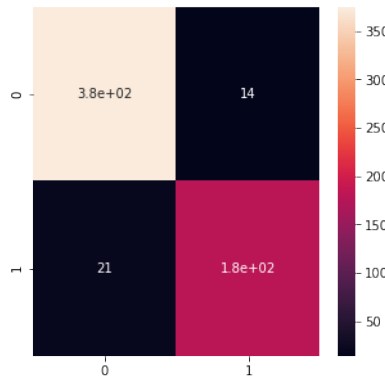


Figure 7 Confusion Matrix of Tumor Recognition and Classification Model

0 indicates that a tumor exists based on the MRI image judged by the model, and 1 indicates that a tumor does not exist based on the MRI image judged by the model. According to the confusion matrix of Figure 7, the prediction indicators in this paper can be obtained as shown in Table 2.

Table 2 Predictive Indexes of ResUNet for MRI

	precision	recall	f1-score	support
0	0.95	0.96	0.96	389
1	0.93	0.90	0.91	201
accuracy			0.94	590
macro avg	0.94	0.93	0.93	590
weighted	0.94	0.94	0.94	590
avg				

It can be seen from Table 2 that the accessibility of ResUNet for MRI classification is 0.94, the macro avg and weighted avg of precision are 0.94, the macro avg and weighted avg of the recall are 0.93 and 0.94 respectively, and the macro avg and weighted avg of f1 value are 0.93 and 0.94 respectively. This shows that ResUNet has a high classification performance for MRI.

3.3 Target Detection and Segmentation

According to the above tumor recognition processing, the image images with tumors are successfully screened out. Here, the ResUNet model structure is designed for target segmentation training, forming a composite network composed of 1,210,513 parameters, excluding 4,384 untrainable parameters, and training with training sets for 1,206,129 trainable parameters. The training process is shown in Figure 8.

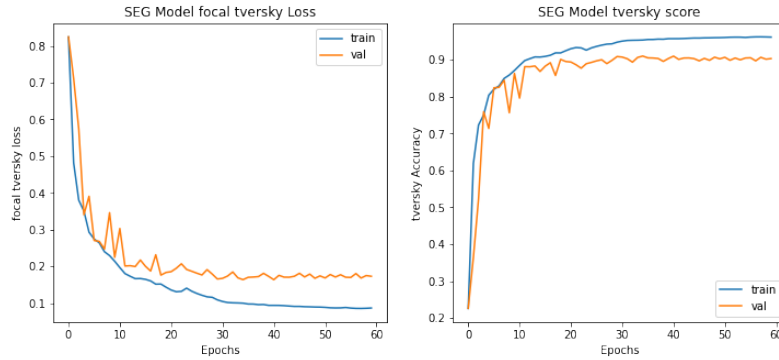


Figure 8 Training Details of Tumor Detection and Segmentation Model

In Figure 8, the training set and the test set are used to train and test the model respectively, obtaining the loss function value and accuracy of ResUNet with the changing number of iterations in the training and testing process. The training results show that after many iterations, the model finally converges with good training accuracy and test accuracy, which are maintained at about 95% and 90% respectively. It is shown that the model can effectively learn and capture the information and features in the data during the training process, thus achieving satisfactory target segmentation without the fitting situation.

To visualize the target segmentation effect of the ResUNet model, some MRI images were randomly selected for display as shown in Figure 9.

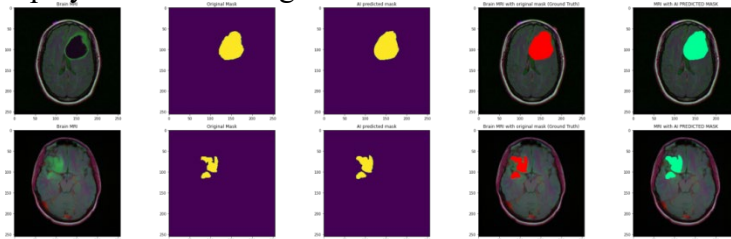


Figure 9 Evaluation Index of Tumor Recognition and Classification Model

According to Figure 9, the first column is the original MRI image, the second is the target area of the artificially calibrated tumor, the third is the target area segmented by the model, and the fourth and fifth are the superimposed enhanced display of the second and third column areas and the original image respectively. It can be seen that the tumor region segmented by the ResUNet model is highly consistent with the artificially calibrated region in this paper with a high learning degree.

FPN [14], U-Net, Res-Net, and ResUNet are used to compare the segmentation performance, and Loss and IoU are used as the evaluation indexes. The comparison of the target segmentation performance of four networks is shown in Table 3.

Table 3 Comparison of Target Segmentation Evaluation Indexes of Four Networks

	Loss	IoU	Dice Coef
FPN	15.89%	92.00%	93.81%
U-Net	19.71%	81.50%	77.57%
Res-Net	17.24%	72.47%	83.82%
ResUNet	13.02%	99.75%	89.69%

It can be seen from Table 3 that ResUNet has higher IoU and lower Loss value than FPN, U-Net, and Res-Net in the MRI segmentation experiment, which shows that ResUNet has a better matching degree for target segmentation than FPN, U-Net, and Res-Net in brain MRI for tumor detection segmentation.

4. Conclusion

This paper studies the recognition and segmentation of brain tumors in MRI images by ResUNet, which was used to recognize brain tumors from LGG-segmented datasets. Meanwhile, ResUNet was used to compare MRI segmentation results with FPN, U-Net, and Res-Net. It is proven that ResUNet

has higher prediction performance for MRI and higher segmentation performance than FPN, U-Net, and ResNet. This study has some research significance and value in clinical application.

References

- [1] Hou, W. N., Wang, L., Chen, F. & Lu, J. (2023). Study on diagnosis and treatment of prostate cancer based on magnetic resonance imaging. *Chinese Journal of Medicine*, 58(06), 583-586.
- [2] Qi, Y. L., Zhao, Q. Q., Cheng, C. L., Zou, C., Liu, X., Zheng, H. R. & Cheng, G. X. (2022). Correlation between body fat distribution characteristics and anthropometric parameters based on magnetic resonance imaging. *Chinese Journal of CT and MRI*, 20(08), 180-185.
- [3] Meng, X. F., Hao, X. L., Mao, C. H. et al. (2023). Research on machine learning for scientific discovery. *Chinese Journal of Computers*, 46(05), 877-895.
- [4] Chen, G. X. (2021). Research on COVID-19 X-ray image recognition method based on deep learning. Chengdu: Dissertation of Master's Degree of Southwest Jiaotong University.
- [5] Zhang, P., Xu, X. N., Wang, H. W. et al. (2018). Computer-aided lung cancer diagnosis approaches based on deep learning. *Journal of Computer-Aided Design & Computer*, 30(01), 90-99.
- [6] Cheng, H., Cai, X., Jiang, X. P. et al. (2023). Overview of under-sampled magnetic resonance image reconstruction based on deep learning. *Software Engineering*, 26(06), 1-5.
- [7] Chen, Z. Z., Chen, X. F., Wang, W. Q. et al. (2023). Application status and development trend of deep learning in lumbar MRI imaging research. *Journal of Clinical Radiology*, 42(02), 345-348. DOI:10.13437/j.cnki.jcr.2023.02.037.
- [8] Xia, Z. Y., Liu, J., Kang, Y. Q. et al. (2023). Low dose CT image processing based on dynamic controllable residual convolution neural network. *Journal of Chongqing Technology and Business University (Natural Science Edition)*, 40(02), 64-72. DOI:10.16055/j.issn.1672-058X.2023.0002.010.
- [9] Ronneberger, O., Fischer, P. & Brox, T. (2015). U-Net: Convolutional networks for biomedical image segmentation. *CoRR*. Volume abs/1505.04597, Issue. 2015.
- [10] Guo, X. M. (2022). Research on CT image-assisted diagnosis technology of pulmonary nodules based on deep learning. Guilin: Guilin University of Electronic Technology.
- [11] Meng, X. H. (2019). Multi-modal image segmentation of brain and abdomen based on improved Unet. Xi'an: Dissertation of Master's Degree of Xidian University.
- [12] Liu, Y., Lu, Z. Y., Wang, J. et al. (2023). Gibbs artifact removal algorithm for magnetic resonance imaging based on self-attention connection UNet. *Journal of Computer Applications*, 43(05), 1606-1611.
- [13] Liang, J. Y., Cao, J. Z., Sun, G. L. et al. (2021). SwinIR: image restoration using Swin Transformer. *Proceedings of the 2021 IEEE/CVF International Conference on Computer Vision Workshops*. IEEE, 1833-1844.
- [14] Lin, T. Y., Dollar, P., Girshick, R. et al. (2017). Feature pyramid networks for object detection. *IEEE Computer Society*, DOI:10.1109/CVPR.2017.106.